Research Article

Downregulation of miR-491-5p promotes neovascularization after traumatic brain injury

https://doi.org/10.4103/1673-5374.314326
Date of submission: January 21, 2021
Date of decision: February 22, 2021
Date of acceptance: March 22, 2021
Date of web publication: August 4, 2021

Wei Tang[1], Zong-Duo Guo[1], Wei-Na Chai[1], Dong-Lin Du[1], Xiao-Min Yang[1], Lang Cao[2], Hong Chen[1], Chao Zhou[1], Chong-Jie Cheng[1], Xiao-Chuan Sun[1], Zhi-Jian Huang[1,*], Jian-Jun Zhong[1,*]

Graphical Abstract *Downregulation of miR-491-5P promotes neovascularization around the injury site after traumatic brain injury*

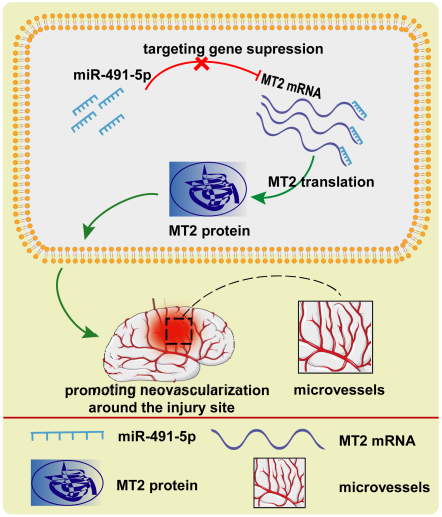

Abstract

MicroRNA-491-5p (miR-491-5p) plays an important role in regulating cell proliferation and migration; however, the effect of miR-491-5p on neovascularization after traumatic brain injury remains poorly understood. In this study, a controlled cortical injury model in C57BL/6 mice and an oxygen-glucose deprivation model in microvascular endothelial cells derived from mouse brain were established to simulate traumatic brain injury *in vivo* and *in vitro*, respectively. In the *in vivo* model, quantitative real-time-polymerase chain reaction results showed that the expression of miR-491-5p increased or decreased following the intracerebroventricular injection of an miR-491-5p agomir or antagomir, respectively, and the expression of miR-491-5p decreased slightly after traumatic brain injury. To detect the neuroprotective effects of miR-491-p, neurological severity scores, Morris water maze test, laser speckle techniques, and immunofluorescence staining were assessed, and the results revealed that miR-491-5p downregulation alleviated neurological dysfunction, promoted the recovery of regional cerebral blood flow, increased the number of lectin-stained microvessels, and increased the survival of neurons after traumatic brain injury. During the *in vitro* experiments, the potential mechanism of miR-491-5p on neovascularization was explored through quantitative real-time-polymerase chain reaction, which showed that miR-491-5p expression increased or decreased in brain microvascular endothelial cells after transfection with an miR-491-5p mimic or inhibitor, respectively. Dual-luciferase reporter and western blot assays verified that metallothionein-2 was a target gene for miR-491-5p. Cell counting kit 8 (CCK-8) assay, flow cytometry, and 2′,7′-dichlorofluorescein diacetate (DCFH-DA) assay results confirmed that the downregulation of miR-491-5p increased brain microvascular endothelial cell viability, reduced cell apoptosis, and alleviated oxidative stress under oxygen-glucose deprivation conditions. Cell scratch assay, Transwell assay, tube formation assay, and western blot assay results demonstrated that miR-491-5p downregulation promoted the migration, proliferation, and tube formation of brain microvascular endothelial cells through a metallothionein-2-dependent hypoxia-inducible factor-1α/vascular endothelial growth factor pathway. These findings confirmed that miR-491-5p downregulation promotes neovascularization, restores cerebral blood flow, and improves the recovery of neurological function after traumatic brain injury. The mechanism may be mediated through a metallothionein-2-dependent hypoxia-inducible factor-1α/vascular endothelial growth factor signaling pathway and the alleviation of oxidative stress. All procedures were approved by Ethics Committee of the First Affiliated Hospital of Chongqing Medical University, China (approval No. 2020-304) on June 22, 2020.

Key Words: brain injury; cell migration; cell proliferation; endothelial cell; hypoxia-inducible factor-1 alpha; metallothionein 2; microRNA; neovascularization; neurons; vascular endothelial growth factor

Chinese Library Classification No. R459.9; R363; R364

[1]Department of Neurosurgery, First Affiliated Hospital of Chongqing Medical University, Chongqing, China; [2]Department of Ophthalmology, First Affiliated Hospital of Chongqing Medical University, Chongqing, China

*__Correspondence to:__ Zhi-Jian Huang, MD, PhD, zhijian@cqmu.edu.cn; Jian-Jun Zhong, MD, PhD, jianjun@hospital.cqmu.edu.cn.
https://orcid.org/0000-0002-8241-0761 (Zhi-Jian Huang); https://orcid.org/0000-0002-9481-5088 (Jian-Jun Zhong)

Funding: *This work was supported by the National Natural Science Foundation of China, Nos. 82071397 (to XCS), 82071332 (to ZDG); the Youth Fund of the National Natural Science Foundation of China, No. 81801230 (to JJZ); and the Excellent Scientific Research Talents Fund of the First Affiliated Hospital of Chongqing Medical University, China (to JJZ).*

How to cite this article: *Tang W, Guo ZD, Chai WN, Du DL, Yang XM, Cao L, Chen H, Zhou C, Cheng CJ, Sun XC, Huang ZJ, Zhong JJ (2022) Downregulation of miR-491-5p promotes neovascularization after traumatic brain injury. Neural Regen Res 17(3):577-586.*

Introduction

Traumatic brain injury (TBI) is a significant public challenge in today's society and becoming the third leading cause of death worldwide by 2020 (Meaney et al., 2014; Jiang et al., 2019; Wang et al., 2021). In recent years, although many studies have examined treatment options after TBI, no available therapeutic method has been confirmed to significantly improve the outcome of TBI patients in clinical practice, which may be due to an incomplete understanding of the pathophysiological mechanisms that underlie TBI.

With further exploration, research focusing on the treatment of TBI has shifted from a focus on neurons alone to including the neurovascular unit (Zhou et al., 2020a, b). In the field of central nervous system disease research, the concept of the neurovascular unit was first suggested as a target for the treatment of stroke and neurodegenerative diseases (Arai et al., 2011; Lecrux and Hamel, 2011). Microvessels, which represent components of the neurovascular unit, become damaged by TBI, disrupting the blood supply and exacerbating neuronal loss at or around the injury site (Guo et al., 2016). Neovascularization could partially reverse this pathological state and alleviate functional neurological damage following TBI (Arai et al., 2011; Huang et al., 2013; Yan et al., 2020). The promotion of neovascularization after TBI represents a new research direction for TBI treatment. A series of biological activities, such as vascular endothelial cell proliferation, migration, and tube formation, are necessary prerequisites for neovascularization to occur (Prakash and Carmichael, 2015; Tiwari et al., 2018; Fukai and Ushio-Fukai, 2020; Zhou et al., 2020a, b). Therefore, promoting these activities in brain microvascular endothelial cells (BMECs) at injury sites following TBI might promote local revascularization. Metallothionein-2 (MT2) has been demonstrated to promote neovascularization, both *in vivo* and *in vitro*, and the mechanism primarily involves the regulation of hypoxia-inducible factor 1α (HIF-1α) and vascular endothelial growth factor (VEGF) expression (Schuermann et al., 2015; Wang et al., 2020). Therefore, increasing the expression of MT2 after TBI may promote neovascularization.

MicroRNAs (miRNAs) are noncoding RNAs composed of 18–23 nucleotides that can restrain the translation or induce the degradation of targeted mRNA molecules by binding the 3'-untranslated region (UTR) of targeted mRNAs (Ved and Zaben, 2018). miRNAs can modulate the pathophysiological process after TBI. For example, miR-9-5p can increase neovascularization after TBI by inhibiting Ptch1 mRNA translation, which activates the Hedgehog pathway (Wu et al., 2020). miR-146a can alleviate TBI through the inhibition of the c-Jun N-terminal kinase (JNK) and nuclear factor kappa B (NF-κB) signaling pathways (Zhang et al., 2020). A previous study confirmed that miRNA-491 inhibits tumor neovascularization by inhibiting the transforming growth factor-beta (TGF-β)/SMAD3/NF-κB pathway and VEGF secretion (Jiang et al., 2014). Conversely, the downregulation of miRNA-491-5p may promote neovascularization. However, the effects of miR-491-5p on neovascularization after TBI require additional investigation.

In this study, an *in vivo* controlled cortical injury (CCI) model and an *in vitro* oxygen-glucose deprivation (OGD) model were established to probe the effects of miR-491-5p on angiogenesis after TBI.

Materials and Methods

Animals

C57BL/6 male mice, weighing 20–25 g and aged 8–12 weeks (n = 112), and 1-week-old mice (both male and female; n = 28) were provided by the Animal Experiment Center of Chongqing Medical University, China (license No. SYXK (Yu) 2018-0003). All mice were housed at the Animal Experiment Center of Chongqing Medical University with a 12-hour dark/light cycle and free access to food and water. All procedures strictly adhered to the guidelines established by the Chongqing Management Approach of Laboratory Animal and were approved by the Ethics Committee of the First Affiliated Hospital of Chongqing Medical University, China (approval No. 2020-304) on June 22, 2020.

The 8–12-week-old mature mice were used to establish the CCI model, whereas the 1-week-old mice were used to extract and culture primary BMECs. The mature mice (n = 112) were randomly divided into four groups. In the sham group (n = 28), mice received a craniotomy but no CCI. In the CCI group (n = 28), mice received CCI. In the CCI + agomir group (n = 28), mice received CCI and miR-491-5p agomir treatment. In the CCI + antagomir group (n = 28), mice received CCI and miR-491-5p antagomir treatment. All the procedures were performed in a double-blinded manner. In the preliminary experiment, we found that agomir and antagomir treatments applied to the sham group had no substantial effects; therefore, we did not include these two groups in the current experimental design. Anesthesia induction was manipulated as described in our previous study (Zhong et al., 2016).

CCI model establishment

A CCI model was generated to mimic TBI in mice. In brief, the mice were anesthetized with 3% isoflurane (Yuyan Instruments, Shanghai, China) in 67% N_2O/30% O_2 and maintained with 1.5% isoflurane (Yuyan Instruments) by inhalation (RWD, Shenzhen, China). A bone flap (3.5 mm) was removed from the lower right junction of Bregma and the coronal suture. The cerebral cortex in the bone window was impacted with an impactor (3 mm). The parameters of the impactor strength were as follows: tissue depth, 2.0 mm; dwell time, 0.1 seconds; and speed, 5.0 m/s (Zhong et al., 2016; Martinez and Peplow, 2017; Zhou et al., 2021). After this procedure was completed, the scalp was sutured, and the mice were allowed to recover in a warm, heated blanket. All procedures were performed by two individuals who were familiar with CCI modeling and in a double-blinded manner.

Intracerebroventricular injection

Either miR-491-5p agomir or antagomir (RiboBio, Guangzhou, China) was injected into the lateral ventricles using a stereotaxic device (Hamilton, Bonaduz, Switzerland) under general anesthesia, based on the protocols described in our previous study (Zhong et al., 2016). Briefly, 5 μL diluted miR-491-5p agomir (1 μM) or antagomir (2 μM) was injected into the right cerebral lateral ventricle at the following coordinates (relative to Bregma) under stereotaxic apparatus guidance: dorsoventral −2 mm, anteroposterior +1.5 mm, and mediolateral +1 mm. Injections were performed 15 minutes post-CCI.

Neurobehavioral tests

Neurobehavior in mice was evaluated according to our previous protocols (Zhong et al., 2017; He et al., 2018). Briefly, the neurological severity score (NSS) was used to evaluate neurological function in mice preoperatively and 1, 3, 7, 14, and 21 days after CCI. The maximum possible score is 10 points. A higher score indicates increased injury severity: severe, > 7 points; moderate, 4–6 points; and mild, 0–3 points. The evaluation was conducted three times at each time point, and the average value of these three assessments was used. Cued learning ability was assessed using the Morris water maze assay, which was performed 16–20 days after TBI. Spatial memory was evaluated by the Morris water maze test 21 days after CCI when the hidden platform was removed. The platform was located in quadrant 4.

Immunofluorescence assay

Immunofluorescence staining was performed 21 days after

TBI, according to our previous protocol (He et al., 2018; Wu et al., 2020). Briefly, the mice were perfused with phosphate-buffered saline (PBS) until the liver turned white, and then the mice were decapitated. The intact brain was removed and fixed in 4% paraformaldehyde and frozen at –80°C. Frozen coronal cerebral cortex sections at the injury site were obtained and cut into consecutive slices. One of every three sections was selected, with a thickness of 15 μm. Three sections were obtained for each mouse for further analyses. Slices were blocked in 5% goat serum and incubated with tetramethylrhodamine (TRITC)-labeled lectin at 37°C for 30 minutes (1:100; Bioss, Beijing, China). 4′6-Diamadino-2-phenylindole (DAPI; Boster, Wuhan, China) was used to stain the cell nuclei. Images were taken under the same imaging parameters (exposure time 400 ms), and three regions of interest were randomly selected in each section (Eclipse Ti-S, Nikon, Tokyo, Japan). The mean fluorescence intensity of lectins per mm2 in three sections of every mouse was recorded and analyzed.

To record the mean number of neurons, coronal cerebral cortex sections (one of every three consecutive sections) were thawed, blocked with 5% goat serum, and incubated with rabbit polyclonal anti-neuronal nuclei (NeuN) antibody (1:400; Cell Signaling Technologies, Danvers, MA, USA) at 4°C overnight, followed by incubation with secondary antibody (Daylights 488 goat anti-rabbit IgG, 1:200; Abbkine, Wuhan, China) at 37°C for 60 minutes. The cell nucleus was stained with DAPI. Three regions of interest were randomly chosen for imaging in each section (Eclipse Ti-S, Nikon), and the mean number of neurons per mm2 was recorded and analyzed.

Cortical blood perfusion assay

Cortical blood perfusion was detected 21 days after TBI using the laser speckle technique, as described in our previous study (Liu et al., 2018). Briefly, the mice were anesthetized with 3% isoflurane (Yuyan Instruments) in 67% N_2O/30% O_2, and anesthesia was maintained using 1.5% isoflurane (Yuyan Instruments) by inhalation (RWD). The scalp and subcutaneous tissues were incised along the sagittal suture, and the parietal bones were exposed on both sides. Cortical blood perfusion changes at the injury site were detected in each group (Perimed, Beijing, China) over a period of time (1 minute). A redder color indicates increased blood perfusion.

Quantitative real time-polymerase chain reaction

TRIzol reagent (TaKaRa, Japan) was applied to extract total RNA from BMEC cultures following OGD model establishment for 24 hours and tissues at 0, 1, 3, 7, 14 and 21 days after TBI (n = 3/group). Quantitative real time-polymerase chain reaction (qRT-PCR) was performed on the Applied Biosystems 7500 Fast System (Thermo Fisher Scientific, Waltham, MA, USA), using the following parameters: 95°C for 2 minutes; 40 cycles of 95°C for 35 seconds, 60°C for 15 seconds, and 72°C for 15 seconds; and 95°C for 15 seconds. The miR-491-5p primer (Forward: 5′-AGT GGG GAA CCC TTC CAT GAG-3′; reverse chain was purchased from TaKaRa, which used a proprietary sequence) was synthesized by Sangon Biotech (Shanghai, China), and miRNA levels were normalized to U6 (forward 5′-GGA ACG ATA CAG AGA TTA GC-3′, reverse: 5′-TGG AAC GCT TCA CGA ATT TGC G-3′) expression levels. The data were calculated using the formula $2^{-\Delta\Delta CT}$.

BMEC culture

BMECs were extracted according to a previously established protocol (Tian et al., 2016). Briefly, 1-week-old mice (n = 28) were anesthetized with 3% isoflurane (Yuyan Instruments) by inhalation (RWD) in 67% N_2O/30% O_2, decapitated, and the meninges removed. The cortex was separated, minced, and digested with 0.25% trypsin at 37°C for 30 minutes and then centrifuged at 800 × g for 10 minutes. Dulbecco's modified Eagle's medium/F12 medium (Gibco, Rockville, MD, USA) containing 20% horse serum was used to resuspend the precipitate, followed by centrifugation at 1680 × g for 10 minutes. Finally, the precipitate was digested at 37°C for 30 minutes, centrifuged at 800 × g for 5 minutes, and resuspended in complete medium (Dulbecco's modified Eagle's medium/F12: fetal bovine serum at 9:1) before seeding.

OGD model establishment

An OGD model was generated with BMECs *in vitro* to mimic the TBI state, as described in previous studies (Tian et al., 2016; Wu et al., 2020). Briefly, after replacing the complete medium with serum-free and glucose-free medium, cells were cultured at 1% O_2, 5% CO_2 and 94% N_2 at 37°C for 24 hours.

MiR-491-5p mimic or inhibitor transfection

MiR-491-5p mimic, miR-491-5p mimic negative control (NC; MIC-NEG), miR-491-5p inhibitor (INH), and miR-491-5p inhibitor-NC (INH-NEG, 100 nM; RiboBio, Guangzhou, China) transfected into BMECs according to the manufacturer's instructions. For solution 1, 10 μL of mimic or inhibitor was mixed with 250 μL Opti-MEM (Gibco, Rockville, MD, USA) and incubated at room temperature for 5 minutes. For solution 2, 5 μL Lipofectamine® 2000 reagent (Invitrogen, Waltham, MA, USA) was mixed with 250 μL Opti-MEM and incubated for 5 minutes. The two solutions were mixed together and incubated at room temperature for 20 minutes. Afterward, the solution was diluted to a final volume of 2 mL with serum-free medium and used to transfect BMECs. After 7 hours of transfection, the transfection medium was replaced with complete medium. The transfection efficiency was tested on the second day after transfection. The transfected cells were used in all subsequent analyses. The NC sequences, MIC-NEG and INH-NEG, are sequences of the same length as the miR-491-5p-mimic and INH that are not found and have no effect in human genes, mouse genes, and rat genes, and were used to indicate that the miR-491-5p-mimic/INH were specific to miR-491-5p.

CCK-8 assay

The cell counting kit 8 (CCK-8) assay (Do Jindo Laboratories, Japan) was performed after 24-hour OGD treatment to determine BMEC viability, according to the manufacturer's instructions. In brief, 2 × 10^3 BMECs were seeded in each well of a 96-well plate and washed three times with serum-free medium after OGD treatment. The CCK-8 working buffer (100 μL) was added to each well and incubated in a cell incubator for 4 hours. A microplate reader (Thermo Fisher Scientific) was used to detect the absorbance at 450 nm. Cell viability was calculated as follows: (sample group – blank group)/ (untreated group – blank group), where the blank group represents the absorbance value of the CCK8 working buffer in the absence of cells.

Cell scratch assay

The cell scratch assay was performed after 24-hour and 48-hour OGD treatment to determine the migration ability of BMECs, as described by a previous study (Wu et al., 2020). Briefly, a confluent BMEC layer in a six-well plate was scratched with a 200-μL pipette tip and washed with PBS to remove cell debris. The BMECs were cultured in serum-free medium under OGD treatment and imaged by microscopy (Leica, Wetzlar, Hesse, Germany) at 0, 24, and 48 hours after the scratch. The migration area (%) was calculated as follows: [cell-free area (0 hour) – cell-free area (24/48 hours)]/[cell-free area (0 hour)] ×100.

Transwell assay

The Transwell assay was used to explore the migration ability of BMECs under OGD treatment for 24 hours. Briefly, 5 × 10^4 BMECs were seeded into the upper chamber after transfection

with miR-491-5p INH or INH-NEG in serum-free medium and 2 mL complete medium under OGD treatment for 24 hours was added to the lower chamber. The cells remaining in the upper chamber were wiped off after treatment, and the cells on the lower surface of the membrane were fixed and stained at room temperature for 5 minutes using 0.1% crystal violet diluted with methanol. Cells were washed and imaged by microscopy (Leica).

Tube formation assay

The tube formation assay was used to determine the tube formation abilities of BMECs after 24-hour OGD treatment, as described by a previous study (Wu et al., 2020). Matrigel (BD Biosciences, Shanghai, China) was diluted with complete medium (4:2), and 50 µL diluted Matrigel was added to 96-well plates and incubated at 37°C for 30 minutes. Then, 1×10^4 BMECs were seeded into each well, treated with OGD for 24 hours, and imaged by microscopy (Leica).

Dual-luciferase reporter assay

The dual-luciferase reporter assay was performed to determine whether miRNAs directly bind to target mRNAs (Sun et al., 2018). Briefly, the predicted wild-type (WT: GGA GGG GTC CCC AC) and mutant (Mut: AGG AAA GCT TTT GT) binding site sequences of MT2 were designed according to the predictions found on the databases miRWalk, miRDB, and ENCORI. The binding site sequences were cloned into the pmirGLO vector. The pGL3-MT2-WT vector, pGL3-MT2-Mut vector, miR-491-5p mimic and MIC-NEG were randomly transfected into 293T cells for 48 hours using four transfection conditions (MIC-NEG + Mt2-WT group, MIC + Mt2-WT group, MIC-NEG + Mt2-Mut group, MIC + Mt2-Mut group), and a chemiluminescent analyzer (Thermo Fisher Scientific) was used to detect luciferase activity.

Western blot assay

Cell lysates (40 µg) were extracted after 24-hour OGD treatment, separated by electrophoresis (Bio-Rad, CA, USA) at 90 V, and transferred to polyvinylidene fluoride membranes (0.45 µm; Millipore, Boston, MA, USA) at 250 mA. The membranes were blocked and incubated at 4°C overnight with primary antibodies: rabbit monoclonal anti-MT2 (1:200, ImmunoClone, Houston, TX, USA); rabbit polyclonal anti-HIF-1α (1:1000), rabbit polyclonal anti-phosphorylated p38-mitogen-activated protein kinase (p-p38MAPK)/rabbit polyclonal anti-p38MAPK (1:1000), rabbit polyclonal anti-phosphorylated extracellular-signal-regulated protein kinase (p-ERK)/ rabbit polyclonal anti-ERK (1:1000; Cell Signaling Technologies); rabbit polyclonal anti-VEGF (1:1000), rabbit polyclonal anti-matrix metalloproteinase 9 (MMP-9; 1:1000), rabbit polyclonal anti-cyclin D1 (1:500) (Proteintech, Wuhan, China); and mouse monoclonal anti-β-actin (1:800, Boster). The membranes were washed and incubated in secondary antibodies (1:5000, Proteintech) at room temperature for 120 minutes and visualized by an enhanced chemiluminescence (ECL) system (Thermo), and analyzed by ImageJ software (NIH, Bethesda, MD, USA) (Zhong et al., 2017; He et al., 2018).

Apoptosis assay using flow cytometry

To detect the apoptosis of BMECs, flow cytometry was performed after 24-hour OGD treatment, as previously described (Bai et al., 2018). Briefly, the cells were collected and resuspended in 500 µL PBS, fixed, and stained with an Annexin V fluorescein isothiocyanate (FITC) apoptosis kit (BD Biosciences, New Jersey, USA). The apoptotic and non-apoptotic cells were separated using a Beckman CytoFLEX (BD Biosciences).

Drug treatment

To explore whether miR-491-5p downregulation promotes neovascularization in an MT2-dependent HIF-1α signaling pathway, LW6 (10 ng/mL), an inhibitor of HIF-1α (Selleck Chemicals, Shanghai, China), was used to inhibit HIF-1α translation (Zhao et al., 2019). BMECs were treated with LW6 for 24 hours before testing.

DCFH-DA assay

A reactive oxygen species (ROS) assay kit (Beyotime Biotechnology, Shanghai, China) was used to assess ROS production in cells. For this assay, 100 µL of serum-free medium containing 2′,7′-dichlorofluorescein diacetate (DCFH-DA) working buffer (1:1000) was added to each well after 24-hour OGD treatment. BMECs were cultured in a cell incubator at 37°C for 20 minutes after treatment, washed, and imaged by confocal microscopy (Nikon; excitation wavelength: 488 nm, emission wavelength: 525 nm), and the fluorescence intensity was quantified by Image-Pro Plus (Media Cybernetics, MD, USA).

Statistical analysis

All experimental results were analyzed using SPSS 19.0 software (IBM, Armonk, NY, USA) and expressed as the mean ± standard deviation (SD). NSS scoring, the expression of miR-491-5p after TBI, and the latency in the Morris water maze assay were analyzed by two-way analysis of variance, followed by Tukey's *post hoc* test (Zhong et al., 2017). The dual-luciferase reporter assay data were analyzed by Student's *t*-test. The remaining results were analyzed by one-way analysis of variance, followed by Tukey's *post hoc* test. Statistical plots were created using GraphPad Prism V5.0 software (GraphPad, San Diego, CA, USA). A value of $P < 0.05$ was considered significant.

Results

miR-491-5p expression decreases after TBI, and the downregulation of miR-491-5p improves neurological outcomes

qRT-PCR was used to detect the expression of miR-491-5p at 0, 1, 3, 7, 14, and 21 days after TBI. Compared with those in the CCI group, miR-491-5p expression levels increased in the CCI + agomir group at 1, 3, 7, 14, and 21 days after TBI (**Figure 1A**), whereas levels decreased in the CCI + antagomir group at 1, 3, 7, and 14 days after TBI (**Figure 1A**). Compared with those in the sham group, the miR-491-5p expression levels in the CCI group decreased 1 and 3 days after TBI (**Figure 1A**). Compared with those in the CCI group, the NSS scores were decreased in the CCI + antagomir group 3, 7, and 14 days after TBI (**Figure 1B**), whereas NSS scores increased in the CCI + agomir group 3, 7, 14, and 21 days after TBI (**Figure 1B**). In the Morris water maze test, performed 17, 18, 19, and 20 days after TBI, compared with the CCI group, the latency in the Morris water maze assay was significantly decreased in the CCI + antagomir group (**Figure 1C**) but increased in the CCI + agomir group (**Figure 1C**). The hidden platform was removed 21 days after TBI, and the duration time and swimming distance spent in quadrant 4 and the times passed over the prior platform location were also significantly decreased in the CCI + agomir group but increased in the CCI + antagomir group (**Figure 1D–F**) compared with those in the CCI group. These results indicated that the downregulation of miR-491-5p promotes the rehabilitation of neurological function in mice after TBI.

Downregulation of miR-491-5p increases the number of microvessels and cerebral blood perfusion surrounding the injury site after TBI in mice

A previous study indicated that miR-491 could play an antitumor role in liver cancer by promoting anti-neovascularization (Jiang et al., 2014). At 21 days after TBI, lectin staining was performed to determine the microvessel density surrounding the injury site. Compared with that in the CCI group, the microvessel density in the antagomir group increased (**Figure 2A**), whereas the microvessel density of the agomir group decreased (**Figure 2A**). These results indicated

that the downregulation of miR-491-5p could promote neovascularization after TBI.

To measure changes in cerebral blood perfusion surrounding the injury site in each group, the laser speckle technique was performed. Compared with that in the CCI group, blood perfusion increased in the antagomir group (**Figure 2B**) and decreased in the agomir group (**Figure 2B**). These results indicated that the downregulation of miR-491-5p promoted the recovery of blood perfusion at or around the injury site after TBI.

Downregulation of miR-491-5p promotes neuronal survival after TBI surrounding the injury site in mice

NeuN staining was used to determine the number of neurons in the injury site 21 days after TBI. Compared with that in the CCI group, the number of neurons increased in the antagomir group after TBI (**Figure 3**) and decreased in the agomir group (**Figure 3**). These results showed that miR-491-5p downregulation promoted neuronal survival after TBI.

Downregulation of miR-491-5p decreases apoptosis, improves cell viability, and alleviates oxidative stress in BMECs following OGD treatment

The OGD model was established in BMECs to simulate TBI-induced vascular injury *in vitro*. The level of miR-491-5p expression decreased under OGD treatment compared with that in the control group (**Figure 4A**). No significant changes in miR-491-5p expression were observed in the MIC-NEG, INH-NEG, or OGD groups. Compared with the effects of MIC-NEG, miR-491-5p mimics increased the expression of miR-491-5p after OGD treatment (**Figure 4A**). Compared with INH-NEG treatment, miR-491-5p INH treatment decreased the expression of miR-491-5p after OGD treatment (**Figure 4A**). Moreover, the downregulation of miR-491-5p following INH treatment increased cell viability compared with the viability observed in following INH-NEG treatment (**Figure 4B**). Flow cytometry was used to measure the apoptosis rate in each group OGD conditions, and the results showed that miR-491-5p INH decreased the cell apoptosis rate compared with INH-NEG (**Figure 4C** and **E**).

ROS levels in cells reflect cellular oxidative stress (Daverey and Agrawal, 2016). The present study showed that OGD treatment increased ROS levels in BMECs compared with those in the control group. However, compared with INH-NEG treatment, miR-491-5p INH treatment decreased ROS levels in BMECs under OGD conditions (**Figure 4D** and **F**).

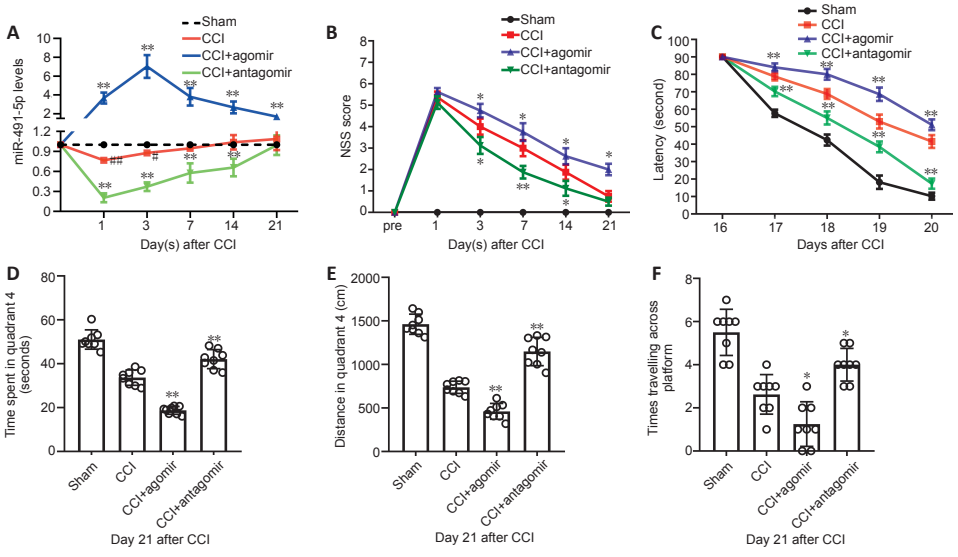

Figure 1 | Downregulation of miR-491-5p improves the recovery of neurological function in mice after TBI.

(A) Quantitative polymerase chain reaction analysis of miR-491-5p levels in the mouse cortex in each group preoperatively and 1, 3, 7, 14, and 21 days after TBI (n = 4). (B) NSS scoring was performed preoperatively and 1, 3, 7, 14, and 21 days after TBI (n = 8). (C) Latency spent in quadrant 4 during the cued learning performance phase of the Morris water maze test 16–20 days after TBI (n = 8). (D) Time spent in quadrant 4 when the platform was removed from the Morris water maze test 21 days after TBI (n = 8). (E) Length of the swimming tracks in quadrant 4 after the platform was removed from the Morris water maze test 21 days after TBI (n = 8). (F) Time traveling across the previous platform location after the platform was removed from the Morris water maze test 21 days after TBI (n = 8). Data are expressed as the mean ± SD (one-way analysis of variance followed by Tukey's *post hoc* test). *P < 0.05, **P < 0.01, *vs.* CCI group; #P < 0.05, ##P < 0.01, *vs.* sham group. CCI: Controlled cortical injury; NSS: neurological severity scores; TBI: traumatic brain injury.

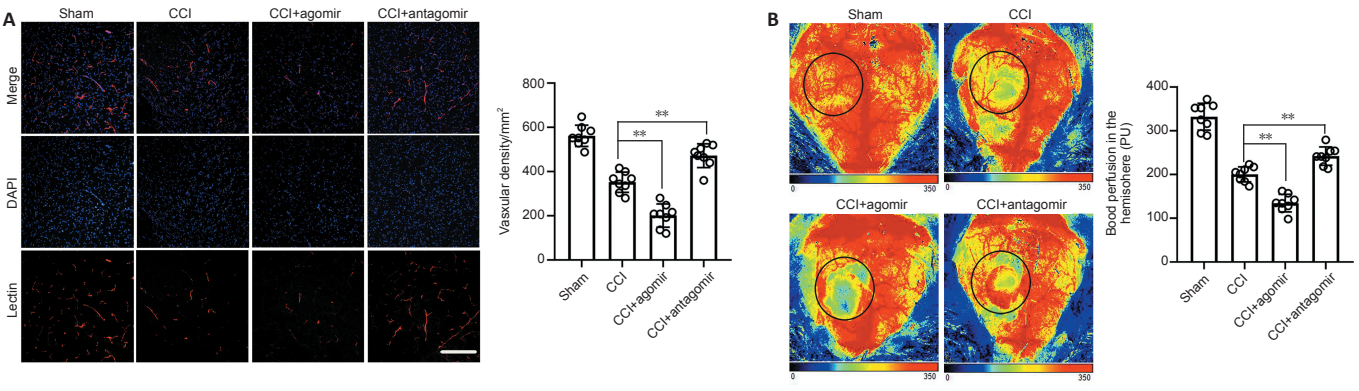

Figure 2 | Downregulation of miR-491-5p promotes neovascularization and the recovery of cerebral blood flow around the injury site 21 days after TBI in mice.

(A) Lectin-positive microvasculature around the injury site after TBI in mice (left) and quantification (right); lectin is a marker of the microvasculature (red); DAPI is a marker of the cell nucleus (blue). Scale bar: 100 μm. (B) Laser speckle images of cortical blood perfusion in each group at or around the injury site after TBI in mice (left) and quantification (right): The intensity of the red signal is proportional to the amount of cerebral blood perfusion; the circle represents the area that we detected. Data are expressed as the mean ± SD (n = 8; one-way analysis of variance followed by Tukey's *post hoc* test). **P < 0.01. CCI: Controlled cortical injury; DAPI: 4′,6-diamidino-2-phenylindole; TBI: traumatic brain injury.

MT2 is a target gene of miR-491-5p

To explore the effects of miR-491-5p in BMECs and the underlying mechanisms, bioinformatics databases (miRWalk, miRDB, and ENCORI) were used to identify the target mRNA for miR-491-5p, which revealed that MT2 was a potential target mRNA for this miRNA (**Figure 5A**). Although other mRNAs, such as plakoglobin (Jup), Holliday junction recognition protein (Hjurp), and neurexin-2, were also potential mRNAs targeted by miR-491-5p, MT2 was examined because it has a demonstrated ability to modulate neovascularization (Pedersen et al., 2009). The dual-luciferase reporter assay indicated that the miR-491-5p mimic decreased luciferase activity in the WT group (**Figure 5B**), suggesting that miR-491-5p binds directly with MT2 mRNA. Furthermore, the miR-491-5p INH increased MT2 protein levels (**Figure 5C** and **D**), which indicated that miR-491-5p downregulation increased MT2 expression. MT2 is a small molecule rich in cysteine, resulting in strong antioxidant activity (Nielsen et al., 2007). A previous study found that MT2 could promote neovascularization by activating HIF-1α (Xue et al., 2012; Wang et al., 2020). miR-491-5p INH treatment also increased HIF-1α expression (**Figure 5C** and **E**). We hypothesize that downregulation of miR-491-5p may promote neovascularization through an MT2-dependent HIF-1α pathway.

Downregulation of miR-491-5p promotes BMEC migration and tube formation through an MT2-dependent HIF-1α pathway

To explore the migration and tube formation abilities of BMECs after treatment, cell scratch, Transwell, and tube formation assays were performed. Treatment with miR-491-5p INH increased the migration area compared with the OGD group at 24 and 48 hours following OGD treatment (**Figure 6A–C**); Treatment with LW6 decreased the migration area compared with the OGD group at 24 and 48 hours following OGD treatment (**Figure 6A–C**); however, the effects of the miR-491-5p INH were reversed by treatment with an HIF-1α inhibitor (LW6) (**Figure 6A–C**). Moreover, compared with the OGD group, the number of migrating cells and tubes was higher in the miR-491-5p INH-treated group (**Figure 6D–G**) and lower in the LW6-treated group (**Figure 6D–G**). The ability of the miR-491-5p INH to promote tube formation and cellular migration was partially reduced by LW6 treatment (**Figure 6D–G**); Compared with the OGD group, the number of tube formations in the LW6-treated group decreased (**Figure 6D–G**). Overall, our results showed that the migration and tube formation abilities of BMECs increased when miR-491-5p expression decreased.

Downregulation of miR-491-5p activates the HIF-1α/VEGF/MAPK pathway by enhancing MT2 expression

HIF-1α promotes angiogenesis by increasing VEGF expression during brain development (Lee et al., 2009; Sun et al., 2010). In turn, VEGF promotes vascular endothelial cell migration and proliferation and tube formation by activating the downstream p38-MAPK and ERK pathways (Koch and Claesson-Welsh, 2012). To explore the mechanism through which miR-491-5p promotes neovascularization, the expression levels of MT2, HIF-1α, VEGF, MMP-9, Cyclin D1, p38-MAPK, and ERK in BMECs were detected under OGD conditions. Compared with the OGD group, the expression of MT2 was significantly increased in the OGD + miR-491-5p INH and OGD + miR-491-5p INH + LW6 groups (**Figure 7A** and **B**), whereas no significant differences were observed in MT2 expression among the OGD, OGD + DMSO, and OGD + LW6 groups. By contrast, compared with those in the OGD group, the expression levels of p-p38MAPK/p38MAPK, p-ERK/ERK, HIF-1α, and VEGF were significantly increased in the INH + OGD group (**Figure 7A**, **C**, **D**, **G**, and **H**). Moreover, compared with the OGD group, the miR-491-5p INH-treated group showed a significant upregulation of MMP-9 and cyclin D1 expression (**Figure 7A**, **C–H**). These positive effects of the miR-491-5p INH were reversed by LW6 treatment, which inhibited the expression of HIF-1α, VEGF, MMP-9, cyclin D1, p-ERK/ERK, and p-p38MAPK/p38MAPK in BMECs (**Figure 7A**, **C–H**). These results indicated that the inhibition of miR-491-5p expression promotes neovascularization in BMECs via an MT2-dependent HIF-1α/VEGF pathway.

Discussion

In our previous study, we demonstrated that TBI induced a decrease in regional cerebral blood flow and the number of microvessels (Liu et al., 2018), which led to the formation of an ischemic penumbra and prevented the removal of metabolic waste and necrotic tissues. Secondary ischemic injury exacerbates secondary brain injury, resulting in excessive inflammation and oxidative stress, which eventually aggravates neuronal apoptosis (McConeghy et al., 2012; Gyoneva and Ransohoff, 2015). Therefore, the restoration of blood perfusion around the injury site after TBI is necessary to prevent the development of secondary ischemic injury (Li et al., 2012; Zhang et al., 2019).

Endothelial cells play an important role in neovascularization, and improving endothelial cell activity might enhance the reconstruction of the microvascular network at or around the TBI site (Wu et al., 2020). Growing evidence indicates that miRNAs play an important role in regulating endothelial cell proliferation and migration (Tiwari et al., 2018), which are key features of neovascularization. For example, the upregulation of miR-148a/b-3p has been found to inhibit neovascularization by binding to the 3′-UTR of neuropilin-1 mRNA (Kim et al., 2019). The inhibition of miR-126 promoted tube formation in human umbilical vein endothelial cells by activating the epidermal growth factor-like protein 7 (EGFL7)/phosphoinositide 3-kinase (PI3K)/protein kinase B (AKT) pathway. Moreover, a previous study demonstrated that the inhibition of miR-491 promoted neovascularization in liver cancer (Jiang et al., 2014). Therefore, we propose a hypothesis in which the downregulation of miR-491-5p promotes neovascularization after TBI.

In this study, the expression of miR-491-5p was found to decrease during the acute phase of TBI, and the downregulation of miR-491-5p promoted the rehabilitation of neurological function after TBI. Furthermore, the downregulation of miR-491-5p increased vascular remodeling, blood perfusion recovery, and neuronal survival after TBI. These results indicated that the downregulation of miR-491-5p might promote neovascularization and neuronal survival after TBI.

MiRNAs are small noncoding RNAs (18–23 bp) that inhibit the translation of target mRNAs by interacting with the 3′-UTR (Tiwari et al., 2018; Chang et al., 2020; Sun et al., 2021; Wu et al., 2021; Zhang et al., 2021). On the basis of bioinformatics data, MT2 was predicted to be one of the genes targeted by miR-491-5p. We confirmed that miR-491-5p could bind to the MT2 3′UTR using a dual-luciferase reporter assay. MT2 is a low-molecular-weight protein with a high cysteine content that binds a large number of heavy metal ions (Zhou et al., 2008; Lynes et al., 2014; Takahashi, 2015; Kim and Kang, 2016; Nakajima et al., 2018), indicating a strong ability to scavenge free radicals. This antioxidant role for MT2 explains why the inhibition of miR-491-5p alleviated OGD-induced oxidative stress. To verify the effects of miR-491-5p on neovascularization and to explore the potential underlying mechanism, BMECS were obtained from 1-week-old mice, and an OGD model was established to mimic the TBI state *in vitro*. Although MT2 has been shown to be involved in the regulation of neovascularization and tissue remodeling during the repair and regeneration phase after central nervous system injury (Pedersen et al., 2009), the mechanisms of these functions have not been elucidated.

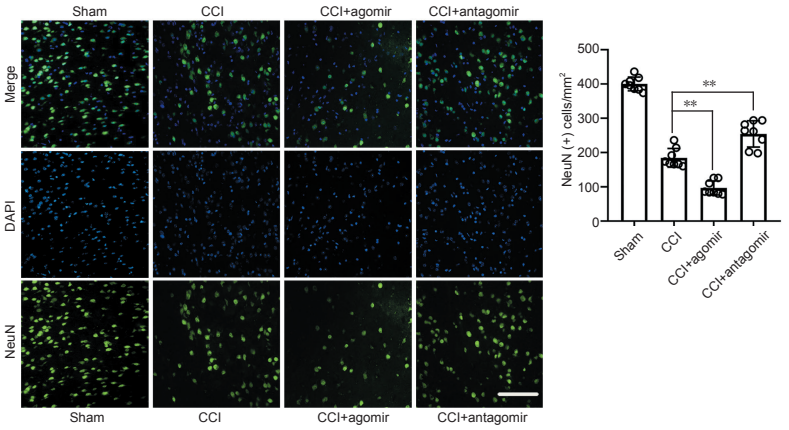

Figure 3 | Downregulation of miR-491-5p promotes neuronal survival around the injury site 21 days after TBI in mice.

NeuN-positive cells around the injury site (left) and quantification (right). NeuN is a marker of neurons (green); DAPI is a marker of cell nuclei (blue). Data are expressed as the mean ± SD (n = 8; one-way analysis of variance followed by Tukey's *post hoc* test). $^{**}P < 0.01$. CCI: Controlled cortical injury; DAPI: 4′,6-diamidino-2-phenylindole; NeuN: neuronal nuclei.

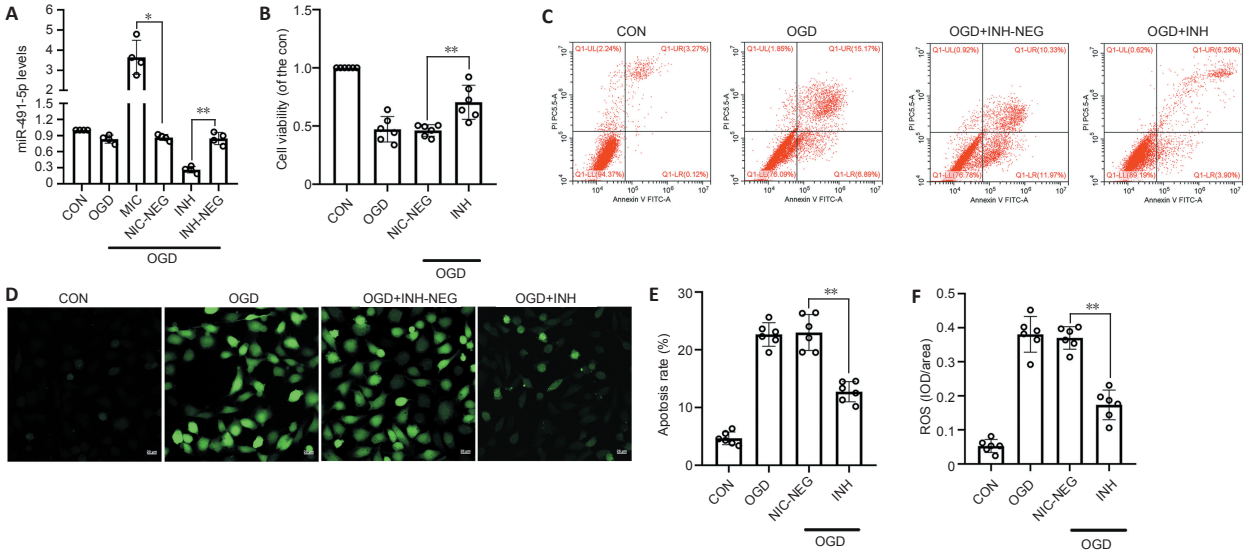

Figure 4 | Downregulation of miR-491-5p improves cell viability, decreases apoptosis, and alleviates oxidative stress.

(A) Quantitative polymerase chain reaction for the detection of miR-491-5p expression levels in each group (n = 4). (B) CCK-8 assay was used to detect cellular viability in each group (n = 6). (C) Flow cytometry was used to detect cell apoptosis in each group and (E) quantified. The lower left quadrant represents normal cells, the lower right quadrant represents early apoptotic cells, the upper right quadrant represents mid-late apoptotic cells, and the upper left quadrant represents necrotic cells (n = 6). (D) ROS levels in each group and (F) quantification: The intensity of green fluorescence is proportional to the level of intracellular oxidative stress (n = 6). Data are expressed as the mean ± SD (one-way analysis of variance followed by Tukey's *post hoc* test). $^{*}P < 0.05$, $^{**}P < 0.01$. INH: MiR-491-5p inhibitor; INH-NEG: miR-491-5p inhibitor negative control; MIC: miR-491-5p mimic; MIC-NEG: miR-491-5p mimic negative control; OGD: oxygen-glucose deprivation; ROS: reactive oxygen species.

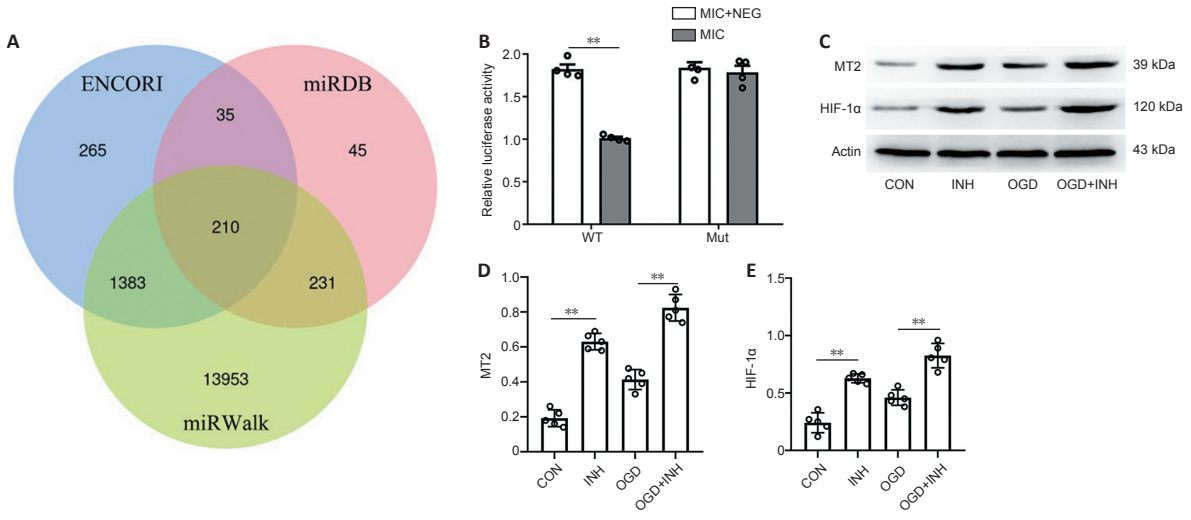

Figure 5 | MT2 is a target mRNA of miR-491-5p, and the downregulation of miR-491-5p increases the expression of MT2.

(A) ENCORI, miRDB, and miRWalk databases were used to predict the target mRNAs of miR-491-5p. (B) The dual-luciferase reporter assay results verified the binding activity between miR-491-5p and the 3′UTR of MT2 mRNA (n = 4). (C) Western blot assay for the detection of MT2 and HIF-1α expression in each group and quantifications: β-actin was used to normalize protein expression levels. (D and E) The ordinates of "MT2" or "HIF-1α" represents the protein expression level of MT2 and HIF-1α (n = 5). Data are expressed as the mean ± SD (B: Student's t-test; D and E: one-way analysis of variance followed by Tukey's *post hoc* test). $^{**}P < 0.01$. HIF-1α: Hypoxia-inducible factor 1α; INH: MiR-491-5p inhibitor; MT2: metallothionein 2; OGD: oxygen-glucose deprivation.

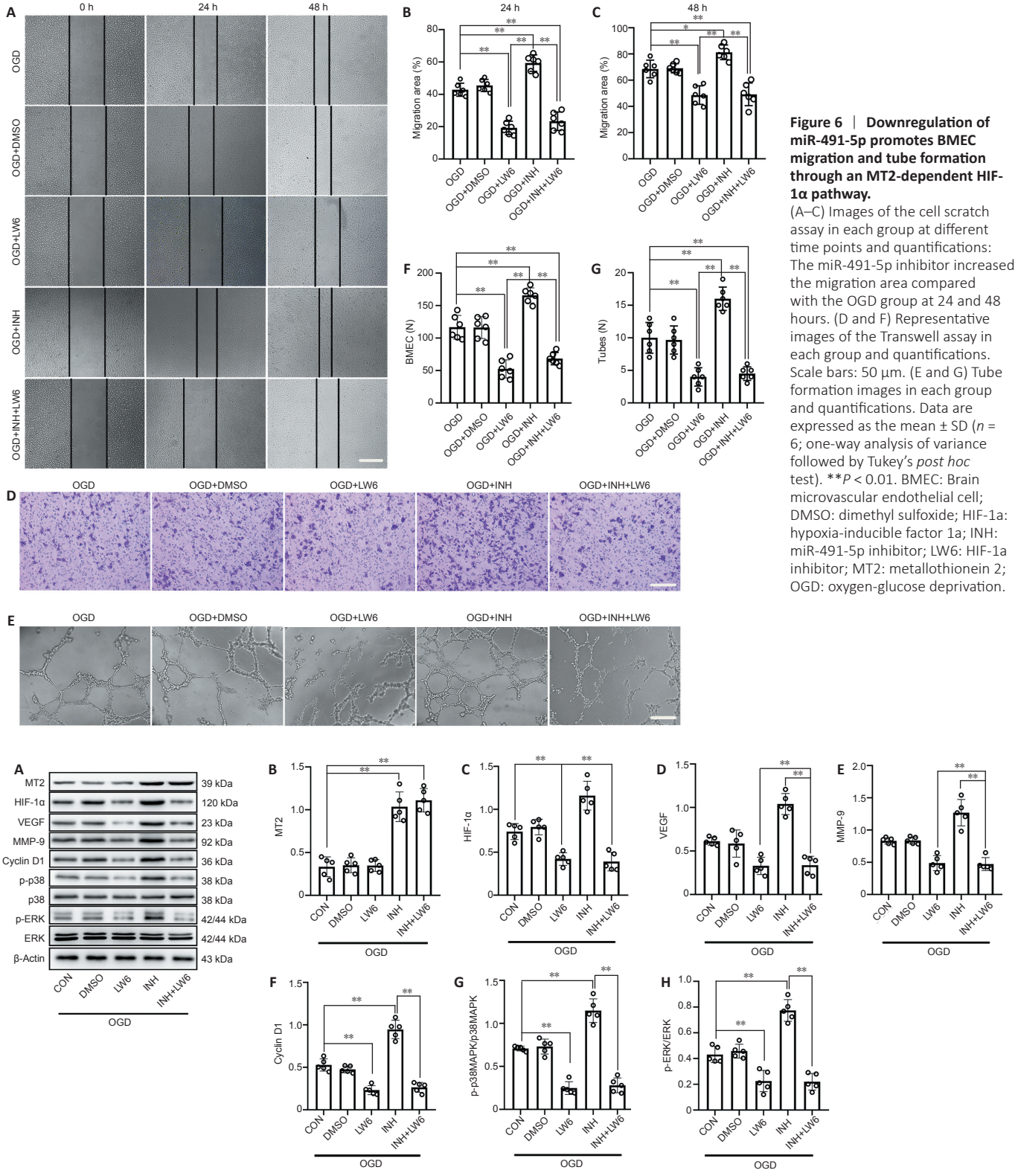

Figure 6 | Downregulation of miR-491-5p promotes BMEC migration and tube formation through an MT2-dependent HIF-1α pathway.

(A–C) Images of the cell scratch assay in each group at different time points and quantifications: The miR-491-5p inhibitor increased the migration area compared with the OGD group at 24 and 48 hours. (D and F) Representative images of the Transwell assay in each group and quantifications. Scale bars: 50 μm. (E and G) Tube formation images in each group and quantifications. Data are expressed as the mean ± SD (n = 6; one-way analysis of variance followed by Tukey's *post hoc* test). $^{**}P < 0.01$. BMEC: Brain microvascular endothelial cell; DMSO: dimethyl sulfoxide; HIF-1a: hypoxia-inducible factor 1a; INH: miR-491-5p inhibitor; LW6: HIF-1a inhibitor; MT2: metallothionein 2; OGD: oxygen-glucose deprivation.

Figure 7 | Downregulation of miR-491-5p activates the HIF-1α/VEGF/MAPK pathway in an MT2-dependent manner.

(A) Western blot assay for the detection of MT2, HIF-1α, VEGF, p-ERK, ERK, p-p38MAPK, p38MAPK, MMP-9, and cyclin D1 protein expression in each group and quantifications (B–H), β-actin was used to normalize the protein expression. Data are expressed as the mean ± SD (n = 5; one-way analysis of variance followed by Tukey's *post hoc* test). $^{**}P < 0.01$. DMSO: Dimethyl sulfoxide; ERK: extracellular-signal-regulated protein kinase; HIF-1α: hypoxia-inducible factor 1α; INH: miR-491-5p inhibitor; LW6: inhibitor of HIF-1α; MMP-9: matrix metalloproteinase-9; OGD: oxygen-glucose deprivation; p38MAPK: p38-mitogen activated protein kinase; p-ERK: phosphorylated extracellular-signal-regulated protein kinase; p-p38MAPK: phosphorylated p38-mitogen activated protein kinase; VEGF: vascular endothelial growth factor.

In a diabetic mouse model of hindlimb ischemia, MT2 overexpression upregulated the HIF-1α/VEGF signaling pathway, promoting the recovery of hindlimb blood flow and neovascularization (Wang et al., 2020). Furthermore, diabetic cardiomyopathy decreased the expression of HIF-1α, which could be rescued by MT2 to promote neovascularization (Xue et al., 2012). MT2 belongs to a family consisting of four primary isoforms (MT1–MT4), which are highly similar, with conserved structures, and perform similar biological functions (Lynes et al., 2014). In this study, the expression of

MT2 and HIF-1α increased in BMECs under OGD conditions following treatment with miR-491-5p INH. MiR-491-5p does not appear to interact with HIF-1α directly, according to the bioinformatics analysis. Therefore, we hypothesized that MT2 might regulate neovascularization via its downstream HIF-1α pathway. The activation of the HIF-1α/VEGF signaling pathway also alleviated damage to BMECs in ischemic stroke disease (Zhang et al., 2018). Therefore, we hypothesized that the downregulation of miR-491-5p promotes neovascularization through an MT2-dependent HIF-1α/VEGF pathway. To verify this hypothesis, LW6 was used to inhibit the HIF-1α pathway. This study demonstrated that the downregulation of miR-491-5p promoted BMEC migration and tube formation, which was partially reversed by LW6. However, the ability of miR-491-5p inhibition to upregulate MT2 expression was not reversed by LW6, indicating that HIF-1α activation occurs downstream of MT2.

Studies have confirmed that VEGF promotes endothelial cell proliferation and migration by activating downstream ERK and p38 MAPK signaling pathways (Koch and Claesson-Welsh, 2012; Chin et al., 2018; Jiang et al., 2020; Watari et al., 2020), which is consistent with the results of our study. The expression levels of VEGF, ERK, and p38 MAPK simultaneously increased in the miR-491-5p INH treatment group. Furthermore, MMP-9, a downstream target of VEGF, promotes neovascularization (Jiang et al., 2020; Wu et al., 2020). Cyclin D1 is a cell cycle regulator and can reflect the proliferation of endothelial cells (Wang et al., 2019; Wu et al., 2020). The downregulation of miR-491-5p also increased the cyclin D1 and MMP-9 expression levels under OGD treatment conditions. The positive effects in BMECS mediated by miR-491-5p downregulation, including the increased expression of HIF-1α, VEGF, p-ERK/ERK, p-p38MAPK/p38MAPK, MMP-9, and cyclin D1, could be blocked by LW6 administration. These results indicated that the downregulation of miR-491-5p promoted neovascularization after TBI through an MT2-dependent HIF-1α/VEGF pathway.

This study had several limitations. First, the OGD model *in vitro* that was used to stimulate a post-TBI state only mimics the ischemic and hypoxic environment of the traumatic foci after TBI. However, ischemia and hypoxia are only parts of the pathophysiological processes that occur following TBI. Therefore, the OGD model might not be the optimal model for the simulation of TBI *in vitro*. Second, previous studies have indicated that miR-491-5p can regulate many genes, in addition to *MT2*, such as *PKM2*, *IGF2*, and *SNAIL* (Chen et al., 2018; Yu et al., 2018; Lu et al., 2019). Our preliminary experiment showed that miR-491-5p were originally expressed in mouse primary cortical neurons and astrocytes without treatment (**Additional Figure 1**). Whether the downregulation of miR-491-5p affects other biological functions or promotes neovascularization through other signaling pathways following TBI remains worthy of further study.

Overall, the downregulation of miR-491-5p promoted neovascularization after TBI, suggesting that this miRNA may represent a therapeutic target for TBI treatment. The mechanism through which the downregulation of miR-491-5p promotes neovascularization after TBI may be mediated by enhanced MT2 expression, which regulates the HIF-1α/VEGF pathway and alleviates oxidative stress.

Acknowledgments: *We express special gratitude to staff from the Chongqing Key Laboratory of Ophthalmology and the Neural Injury and Neuroprotection Laboratory for providing the experimental platform.*
Author contributions: *Study conception and design: WT and JJZ; literature search: WT, CZ, ZDG; experiment performing: WT, DLD, XMY, LC and HC; data collection and analysis: WT, ZDG, WNC, XMY and CJC; manuscript preparation and editing: WT; manuscript review: XCS, ZJH and JJZ; study direction: JJZ and ZJH. All authors approved the final version of this paper.*
Conflicts of interest: *The authors declare no conflict of interest*
Financial support: *This work was supported by the National Natural Science Foundation of China, Nos. 82071397 (to XCS), 82071332 (to ZDG); the Youth Fund of the National Natural Science Foundation of China, No. 81801230 (to JJZ); and the Excellent Scientific Research Talents Fund of the First Affiliated Hospital of Chongqing Medical University, China (to JJZ). The funding sources had no role in study conception and design, data analysis or interpretation, paper writing or deciding to submit this paper for publication.*
Institutional review board statement: *All procedures strictly followed the rules of Chongqing Management Approach of Laboratory Animal approved by the First Affiliated Hospital of Chongqing Medical University, China (approval No. 2020-304) on June 22, 2020. The experimental procedure followed the United States National Institutes of Health Guide for the Care and Use of Laboratory Animals (NIH Publication No. 85-23, revised 1996).*
Copyright license agreement: *The Copyright License Agreement has been signed by all authors before publication.*
Data sharing statement: *Datasets analyzed during the current study are available from the corresponding author on reasonable request.*
Plagiarism check: *Checked twice by iThenticate.*
Peer review: *Externally peer reviewed.*

Additional file:
Additional Figure 1: *The expression of miR-491-5p in mouse primary cortical neuron and astrocytes after cultured 72 hours*

References

Arai K, Lok J, Guo S, Hayakawa K, Xing C, Lo EH (2011) Cellular mechanisms of neurovascular damage and repair after stroke. J Child Neurol 26:1193-1198.
Bai X, Geng J, Li X, Wan J, Liu J, Zhou Z, Liu X (2018) Long noncoding RNA LINC01619 regulates MicroRNA-27a/Forkhead Box protein O1 and endoplasmic reticulum stress-mediated podocyte injury in diabetic nephropathy. Antioxid Redox Signal 29:355-376.
Chang Y, Jin H, Li H, Ma J, Zheng Z, Sun B, Lyu Y, Lin M, Zhao H, Shen L, Zhang R, Wu S, Lin W, Lu Y, Xie Q, Zhang G, Huang X, Huang H (2020) MiRNA-516a promotes bladder cancer metastasis by inhibiting MMP9 protein degradation via the AKT/FOXO3A/SMURF1 axis. Clin Transl Med 10:e263.
Chen T, Li Y, Cao W, Liu Y (2018) miR-491-5p inhibits osteosarcoma cell proliferation by targeting PKM2. Oncol Lett 16:6472-6478.
Chin HK, Horng CT, Liu YS, Lu CC, Su CY, Chen PS, Chiu HY, Tsai FJ, Shieh PC, Yang JS (2018) Kaempferol inhibits angiogenic ability by targeting VEGF receptor-2 and downregulating the PI3K/AKT, MEK and ERK pathways in VEGF-stimulated human umbilical vein endothelial cells. Oncol Rep 39:2351-2357.
Daverey A, Agrawal SK (2016) Curcumin alleviates oxidative stress and mitochondrial dysfunction in astrocytes. Neuroscience 333:92-103.
Fukai T, Ushio-Fukai M (2020) Cross-talk between NADPH oxidase and mitochondria: role in ROS signaling and angiogenesis. Cells 9:1849.
Guo S, Lok J, Zhao S, Leung W, Som AT, Hayakawa K, Wang Q, Xing C, Wang X, Ji X, Zhou Y, Lo EH (2016) Effects of controlled cortical impact on the mouse brain vasculome. J Neurotrauma 33:1303-1316.
Gyoneva S, Ransohoff RM (2015) Inflammatory reaction after traumatic brain injury: therapeutic potential of targeting cell-cell communication by chemokines. Trends Pharmacol Sci 36:471-480.
He J, Liu H, Zhong J, Guo Z, Wu J, Zhang H, Huang Z, Jiang L, Li H, Zhang Z, Liu L, Wu Y, Qi L, Sun X, Cheng C (2018) Bexarotene protects against neurotoxicity partially through a PPARgamma-dependent mechanism in mice following traumatic brain injury. Neurobiol Dis 117:114-124.
Huang XT, Zhang YQ, Li SJ, Li SH, Tang Q, Wang ZT, Dong JF, Zhang JN (2013) Intracerebroventricular transplantation of ex vivo expanded endothelial colony-forming cells restores blood-brain barrier integrity and promotes angiogenesis of mice with traumatic brain injury. J Neurotrauma 30:2080-2088.
Jiang F, Wang X, Liu Q, Shen J, Li Z, Li Y, Zhang J (2014) Inhibition of TGF-beta/SMAD3/NF-kappaB signaling by microRNA-491 is involved in arsenic trioxide-induced anti-angiogenesis in hepatocellular carcinoma cells. Toxicol Lett 231:55-61.

Jiang JH, Pi J, Cai JY (2020) Oridonin exhibits anti-angiogenic activity in human umbilical vein endothelial cells by inhibiting VEGF-induced VEGFR-2 signaling pathway. Pathol Res Pract 216:153031.
Jiang JY, Gao GY, Feng JF, Mao Q, Chen LG, Yang XF, Liu JF, Wang YH, Qiu BH, Huang XJ (2019) Traumatic brain injury in China. Lancet Neurol 18:286-295.
Kim H, Ko Y, Park H, Zhang H, Jeong Y, Kim Y, Noh M, Park S, Kim YM, Kwon YG (2019) MicroRNA-148a/b-3p regulates angiogenesis by targeting neuropilin-1 in endothelial cells. Exp Mol Med 51:1-11.
Kim JH, Kang JC (2016) Oxidative stress, neurotoxicity, and metallothionein (MT) gene expression in juvenile rock fish Sebastes schlegelii under the different levels of dietary chromium (Cr(6+)) exposure. Ecotoxicol Environ saf 125:78-84.
Koch S, Claesson-Welsh L (2012) Signal transduction by vascular endothelial growth factor receptors. Cold Spring Harb Perspect Med 2:a006502.
Lecrux C, Hamel E (2011) The neurovascular unit in brain function and disease. Acta Physiol 203:47-59.
Lee SH, Kim MH, Han HJ (2009) Arachidonic acid potentiates hypoxia-induced VEGF expression in mouse embryonic stem cells: involvement of Notch, Wnt, and HIF-1alpha. Am J Physiol Cell Physiol 297:C207-C216.
Li S, Wei M, Zhou Z, Wang B, Zhao X, Zhang J (2012) SDF-1alpha induces angiogenesis after traumatic brain injury. Brain Res 1444:76-86.
Liu H, He J, Zhang Z, Liu L, Huo G, Sun X, Cheng C (2018) Evolution of cerebral perfusion in the peri-contusional cortex in mice revealed by in vivo laser speckle imaging after traumatic brain injury. Brain Res 1700:118-125.
Lu L, Cai M, Peng M, Wang F, Zhai X (2019) miR-491-5p functions as a tumor suppressor by targeting IGF2 in colorectal cancer. Cancer Manag Res 11:1805-1816.
Lynes MA, Hidalgo J, Manso Y, Devisscher L, Laukens D, Lawrence DA (2014) Metallothionein and stress combine to affect multiple organ systems. Cell Stress Chaperones 19:605-611.
Martinez B, Peplow PV (2017) MicroRNAs as diagnostic markers and therapeutic targets for traumatic brain injury. Neural Regen Res 12:1749-1761.
McConeghy KW, Hatton J, Hughes L, Cook AM (2012) A review of neuroprotection pharmacology and therapies in patients with acute traumatic brain injury. CNS Drugs 26:613-636.
Meaney DF, Morrison B, Bass CD (2014) The mechanics of traumatic brain injury: a review of what we know and what we need to know for reducing its societal burden. J Biomech Eng 136:021008.
Nakajima K, Tanaka T, Masubuchi Y, Ito Y, Kikuchi S, Woo GH, Yoshida T, Shibutani M (2018) Developmental exposure of mice to T-2 toxin increases astrocytes and hippocampal neural stem cells expressing metallothionein. Neurotox Res 35:668-683.
Nielsen AE, Bohr A, Penkowa M (2007) The balance between life and death of cells: roles of metallothioneins. Biomark Insights 1:99-111.
Pedersen MO, Jensen R, Pedersen DS, Skjolding AD, Hempel C, Maretty L, Penkowa M (2009) Metallothionein-I+II in neuroprotection. Biofactors 35:315-325.
Prakash R, Carmichael ST (2015) Blood-brain barrier breakdown and neovascularization processes after stroke and traumatic brain injury. Curr Opin Neurol 28:556-564.
Schuermann A, Helker CS, Herzog W (2015) Metallothionein 2 regulates endothelial cell migration through transcriptional regulation of vegfc expression. Angiogenesis 18:463-475.
Sun J, Sha B, Zhou W, Yang Y (2010) VEGF-mediated angiogenesis stimulates neural stem cell proliferation and differentiation in the premature brain. Biochem Biophys Res Common 394:146-152.
Sun W, Wang X, Li J, You C, Lu P, Feng H, Kong Y, Zhang H, Liu Y, Jiao R, Chen X, Ba Y (2018) MicroRNA-181a promotes angiogenesis in colorectal cancer by targeting SRCIN1 to promote the SRC/VEGF signaling pathway. Cell Death Dis 9:438.
Sun Y, Zhou Y, Shi Y, Zhang Y, Liu K, Liang R, Sun P, Chang X, Tang W, Zhang Y, Li J, Wang S, Zhu Y, Han X (2021) Expression of miRNA-29 in pancreatic beta cells promotes inflammation and diabetes via TRAF3. Cell Rep 34:108576.
Takahashi S (2015) Positive and negative regulators of the metallothionein gene (review). Mol Med Rep 12:795-799.
Tian X, Peng J, Zhong J, Yang M, Pang J, Lou J, Li M, An R, Zhang Q, Xu L, Dong Z (2016) beta-Caryophyllene protects in vitro neurovascular unit against oxygen-glucose deprivation and re-oxygenation-induced injury. J Neurochem 139:757-768.
Tiwari A, Mukherjee B, Dixit M (2018) MicroRNA key to angiogenesis regulation: MiRNA biology and therapy. Curr Cancer Drug Targets 18:266-277.
Ved R, Zaben M (2018) Biomarkers for traumatic brain injury. J Neurol 265:1241-1243.
Wang C, Wang B, Wang B, Wang Q, Liu G, Fan C, Zhang L (2019) A novel granulin homologue isolated from the jellyfish Cyanea capillata promotes proliferation and migration of human umbilical vein endothelial cells through the ERK1/2-signaling pathway. Int J Biol Macromol 135:212-225.
Wang J, Hou Y, Zhang L, Liu M, Zhao J, Zhang Z, Ma Y, Hou W (2021) Estrogen attenuates traumatic brain injury by inhibiting the activation of microglia and astrocyte-mediated neuroinflammatory responses. Mol Neurobiol 58:1052-1061.
Wang K, Dai X, He J, Yan X, Yang C, Fan X, Sun S, Chen J, Xu J, Deng Z, Fan J, Yuan X, Liu H, Carlson EC, Shen F, Wintergerst KA, Conklin DJ, Epstein PN, Lu C, Tan Y (2020) Endothelial overexpression of metallothionein prevents diabetes-induced impairment in ischemia angiogenesis through preservation of HIF-1alpha/SDF-1/VEGF signaling in endothelial progenitor cells. Diabetes 69:1779-1792.
Watari K, Shibata T, Fujita H, Shinoda A, Murakami Y, Abe H, Kawahara A, Ito H, Akiba J, Yoshida S, Kuwano M, Ono M (2020) NDRG1 activates VEGF-A-induced angiogenesis through PLCgamma1/ERK signaling in mouse vascular endothelial cells. Commun Biol 3:107.
Wu G, Zhang J, Fan GG, Zou ZY, Yin YL, Li GX (2021) MiRNA-324-5p inhibits inflammatory response of diabetic vessels by targeting CPT1A. Eur Rev Med Pharmacol 24:12836-12843.
Wu J, He J, Tian X, Li H, Wen Y, Shao Q, Cheng C, Wang G, Sun X (2020) Upregulation of miRNA-9-5p promotes angiogenesis after traumatic brain injury by inhibiting Ptch-1. Neuroscience 440:160-174.
Xue W, Liu Y, Zhao J, Cai L, Li X, Feng W (2012) Activation of HIF-1 by metallothionein contributes to cardiac protection in the diabetic heart. Am J Physiol Heart Circ Physiol 302:H2528-2535.
Yan C, Zhou Y, Chen Q, Luo Y, Zhang JH, Huang H, Shao A (2020) Dysfunction of the neurovascular unit in diabetes-related neurodegeneration. Biomed Pharmacother 131:110656.
Yu T, Wang LN, Li W, Zuo QF, Li MM, Zou QM, Xiao B (2018) Downregulation of miR-491-5p promotes gastric cancer metastasis by regulating SNAIL and FGFR4. Cancer Sci 109:1393-1403.
Zhang B, Zhu X, Wang L, Hao S, Xu X, Niu F, He W, Liu B (2019) Dexamethasone impairs neurofunctional recovery in rats following traumatic brain injury by reducing circulating endothelial progenitor cells and angiogenesis. Brain Res 1725:146469.
Zhang D, Cai G, Liu K, Zhuang Z, Jia K, Pei S, Wang X, Wang H, Xu S, Cui C, Sun M, Guo S, Song W, Cai G (2021) Microglia exosomal miRNA-137 attenuates ischemic brain injury through targeting Notch1. Aging 13:4079-4095.
Zhang L, Luo X, Chen F, Yuan W, Xiao X, Zhang X, Dong Y, Zhang Y, Liu Y (2018) LncRNA SNHG1 regulates cerebrovascular pathologies as a competing endogenous RNA through HIF-1alpha/VEGF signaling in ischemic stroke. J Cell Biochem 119:5460-5472.
Zhang L, Zhao L, Zhu W, Ding Y, Chen H, Chi N (2020) miR-146a mimics ameliorates traumatic brain injury involving JNK and NF-kappaB signaling pathway. Neuromolecular Med 22:484-492.
Zhao B, Liu K, Cai L (2019) LINK-A lncRNA functions in the metastasis of osteosarcoma by upregulating HIF1alpha. Oncol Lett 17:5005-5011.
Zhong J, Jiang L, Cheng C, Huang Z, Zhang H, Liu H, He J, Cao F, Peng J, Jiang Y, Sun X (2016) Altered expression of long noncoding RNA and mRNA in mouse cortex after traumatic brain injury. Brain Res 1646:589-600.
Zhong J, Jiang L, Huang Z, Zhang H, Cheng C, Liu H, He J, Wu J, Darwazeh R, Wu Y, Sun X (2017) The long noncoding RNA Neat1 is an important mediator of the therapeutic effect of bexarotene on traumatic brain injury in mice. Brain Behav Immun 65:183-194.
Zhou C, Chen H, Zheng JF, Guo ZD, Huang ZJ, Wu Y, Zhong JJ, Sun XC, Cheng CJ (2021) Pentraxin 3 contributes to neurogenesis after traumatic brain injury in mice. Neural Regen Res 15:2318-2326.
Zhou F, Liu F, Liu J, He YL, Zhou QM, Guo L, Peng C, Xiong L (2020a) Stachydrine promotes angiogenesis by regulating the VEGFR2/MEK/ERK and mitochondrial-mediated apoptosis signaling pathways in human umbilical vein endothelial cells. Biomed Pharmacother 131:110724.
Zhou G, Li X, Hein DW, Xiang X, Marshall JP, Prabhu SD, Cai L (2008) Metallothionein suppresses angiotensin II-induced nicotinamide adenine dinucleotide phosphate oxidase activation, nitrosative stress, apoptosis, and pathological remodeling in the diabetic heart. J Am Coll Cardiol 52:655-666.
Zhou Y, Chen Q, Wang Y, Wu H, Xu W, Pan Y, Gao S, Dong X, Zhang JH, Shao A (2020b) Persistent neurovascular unit dysfunction: pathophysiological substrate and trigger for late-onset neurodegeneration after traumatic brain injury. Front Neurosci 14:581.

C-Editor: Zhao M; S-Editors: Wang J, Li CH; L-Editors: Giles L, Frenchman B, Qiu Y, Song LP; T-Editor: Jia Y

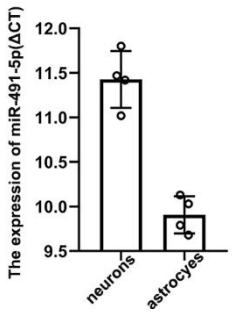

Additional Figure 1 The expression of miR-491-5p in mouse primary cortical neuron and astrocytes after cultured 72 hours

qRT-PCR was used to detect the expression of miR-491-5p in the mouse primary cortical neurons and astrocytes without treatment, U6 was used to normalize the miR-491-5p, the expression of miR-491-5p= miR-491-5p (CT) - U6 (CT) (mean ± SD, n = 4, Student t-test).